Noncovalent Interactions of Zn+ with N-Donor Ligands (Pyridine, 4,4 '-Dipyridyl, 2,2 '-Dipyridyl, and 1,10-Phenanthroline): Collision-Induced Dissociation and Theoretical Studies

ARTICLE *in* THE JOURNAL OF PHYSICAL CHEMISTRY A · FEBRUARY 2012

Impact Factor: 2.69 · DOI: 10.1021/jp207144b · Source: PubMed

2 AUTHORS:

Nalaka Rannulu
University of California, Los Angeles
9 PUBLICATIONS **124** CITATIONS
SEE PROFILE

Mary T Rodgers
Wayne State University
125 PUBLICATIONS **4,182** CITATIONS
SEE PROFILE

THE JOURNAL OF PHYSICAL CHEMISTRY A

Article

pubs.acs.org/JPCA

Noncovalent Interactions of Zn^+ with *N*-Donor Ligands (Pyridine, 4,4′-Dipyridyl, 2,2′-Dipyridyl, and 1,10-Phenanthroline): Collision-Induced Dissociation and Theoretical Studies

N. S. Rannulu and M. T. Rodgers*

Department of Chemistry, Wayne State University, Detroit, Michigan 48202, United States

Supporting Information

ABSTRACT: The binding interactions in complexes of Zn^+ with nitrogen donor ligands, (*N*-L) = pyridine (x = 1−4), 4,4′-dipyridyl (x = 1−3), 2,2′-dipyridyl (x = 1−2), and 1,10-phenanthroline (x = 1−2), are examined in detail. The bond dissociation energies (BDEs) for loss of an intact ligand from the $Zn^+(N\text{-L})_x$ complexes are reported. Experimental BDEs are obtained from thermochemical analyses of the threshold regions of the collision-induced dissociation cross sections of $Zn^+(N\text{-L})_x$ complexes. Density functional theory calculations at the B3LYP/6-31G* level of theory are performed to determine stable structures of these species and to provide molecular parameters needed for the thermochemical analysis of experimental data. Relative stabilities of the various conformations of these *N*-donor ligands and their complexes to Zn^+ as well as theoretical BDEs are determined from single point energy calculations at the B3LYP/6-311+G(2d,2p) and M06/6-311+G(2d,2p) levels of theory using the B3LYP/6-31G* optimized geometries. The experimental BDEs for the $Zn^+(N\text{-L})_x$ complexes are in reasonably good agreement with values derived from density functional theory calculations. BDEs derived from M06 calculations provide better agreement with the measured values than those based on B3LYP calculations. Trends in the sequential BDEs are explained in terms of sp polarization of Zn^+ and repulsive ligand−ligand interactions. Comparisons are made to the analogous $Cu^+(N\text{-L})_x$ and $Ni^+(N\text{-L})_x$ complexes previously studied.

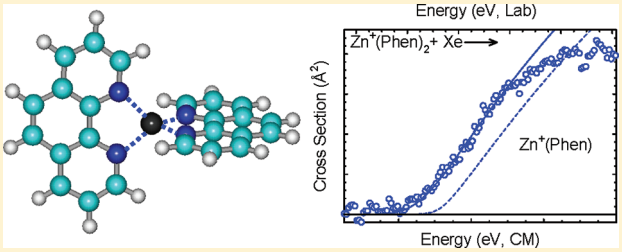

INTRODUCTION

In recent work we have examined the interaction of polypyridyl ligands, 2,2′-dipyridyl and 1,10-phenanthroline, with the late transition metal ions, Cu^+ and Ni^+, to investigate the influence that chelation and the electron configuration of the metal ion have upon the structures and strength of binding.[1,2] In the present study, we extend our investigations to include Zn^+ to examine differences in the nature of the binding resulting from the variation in the valence electron configuration and because of the important applications of zinc dipyridyl complexes reported in the literature. The two nitrogen atoms of these ligands offer chelation to the metal ion via σ donation and π back donation, thereby making them attractive ligands for a wide variety of chemical and technological applications. Earlier studies have found chelation via both nitrogen atoms to be the preferred binding modes of these ligands.

Studies of the interactions of zinc ions with *N*-donor chelating ligands such as 2,2′-dipyridyl and 1,10-phenanthroline have been described in the literature in the development of π conjugated polymers, where metal ion chelation can be used to tune the optical and electronic properties of the material.[3−6] Copolymers of poly(phenylenevinylene) (PPV) and polyfluorene (PF) containing 2,2′-dipyridyl and 1,10-phenanthroline ligands exhibit a strong ionochromic effect such that these materials provide a new approach to sensitive, selective, and highly reversible ion-responsive polymers for metal ion sensors.[7−9] Most metal ions quench the fluorescence of polymers. However, complexation by zinc ions leads to an increase in the photoluminescence quantum yields[10] and alters the emission colors.[11] While the above studies deal with zinc in its most common oxidation state, +2, Zn has also been found in the +1 oxidation state in compounds.[12−14]

In the current study, we examine the interaction of Zn^+ with multiple ligands of pyridine, 4,4′-dipyridyl, 2,2′-dipyridyl, and 1,10-phenanthroline. The structures of these neutral *N*-donor ligands are shown in Figure 1 along with their calculated and measured dipole moments and molecular polarizabilities.[1,15] Collision-induced dissociation (CID) of these complexes is studied using guided ion beam tandem mass spectrometry techniques. The kinetic energy dependent cross sections for the low-energy CID processes are analyzed using methods developed previously.[16] The analysis explicitly includes the effects of the internal and translational energy distributions of the reactants, multiple ion−neutral collisions, and the lifetimes for dissociation. We derive $(N\text{-L})_{x-1}Zn^+\text{−}(N\text{-L})$ bond dissociation energies (BDEs) and compare these results to values obtained from density functional theory calculations performed here. Comparisons of the binding interactions of the

Received: July 27, 2011
Revised: January 4, 2012
Published: January 5, 2012

dx.doi.org/10.1021/jp207144b | J. Phys. Chem. A 2012, 116, 1319−1332

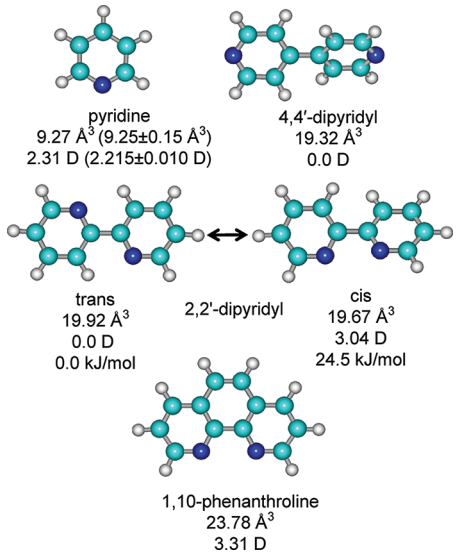

Figure 1. B3LYP/6-31G* optimized geometries of neutral pyridine, 4,4′-dipyridyl, 2,2′-dipyridyl, and 1,10-phenanthroline. Theoretical (and experimental)[12] dipole moments and isotropic molecular polarizabilities are also listed. B3LYP/6-311+G(2d,2p) relative energies of the cis and trans conformers of 2,2′-dipyridyl are taken from our earlier work.[1]

monodentate ligands (pyridine and 4,4′-dipyridyl) with the chelating ligands (2,2′-dipyridyl and 1,10-phenanthroline) are employed to gain a better understanding of the influence that the number and orientation of the donor atoms, and the size and flexibility of the ligands, have upon the binding interactions. Subsequently, trends in the sequential BDEs and total BDEs of these $Zn^+(N\text{-L})_x$ complexes provide a more detailed understanding of the binding in these systems. Comparisons are made to the analogous $Cu^+(N\text{-L})_x$ and $Ni^+(N\text{-L})_x$ complexes previously studied[1,2] to examine the influence of the valence electronic configuration of the metal ion on the structure and strength of binding in these complexes. Ongoing studies of the analogous complexes in their +2 oxidation states will also allow the influence of the charge/oxidation state of the metal ion on the binding interactions to be elucidated.

EXPERIMENTAL SECTION

General Procedures. A guided ion beam tandem mass spectrometer that has previously been described in detail[17] was used to measure absolute CID cross sections of 11 $Zn^+(N\text{-L})_x$ complexes. Zn^+ ions are generated by glow discharge via Ar^+ sputtering of a zinc boat operated at ∼2−4 kV and ∼15−30 mA. The $Zn^+(N\text{-L})_x$ complexes are generated by condensation of Zn^+ with one or more neutral (*N*-L) ligands in a 1.2 m long flow tube ion source operated at 0.5−0.7 Torr pressure. The solid (*N*-L) ligands are introduced into the flow tube by thermal vaporization, while the liquid ligands are introduced using a needle leak valve. The $Zn^+(N\text{-L})_x$ complexes are collisionally stabilized and thermalized by >10^5 collisions with the He and Ar bath gases such that the internal energies of the ions emanating from the source region are assumed to be well described by a Maxwell−Boltzmann distribution at room temperature. The ions are effusively sampled from the source, focused, accelerated, and focused into a magnetic sector momentum analyzer for mass analysis. Mass-selected ions are decelerated to a desired kinetic energy and focused into an octopole ion beam guide. The octopole passes through a static gas cell containing Xe at low pressure (∼0.05−0.20 mTorr), to ensure that multiple ion−neutral collisions are improbable. The octopole ion guide acts as an efficient trap for ions in the radial direction. Therefore, loss of scattered reactant and product ions in the octopole region is almost entirely eliminated.[18] Xe is used here, and in general for all of our CID measurements, because it is heavy and polarizable and therefore leads to more efficient kinetic to internal energy transfer in the CID process.[19−21] Product and unreacted beam ions drift to the end of the octopole, where they are focused into a quadrupole mass filter for mass analysis and subsequently detected with a secondary electron scintillation detector and standard pulse counting techniques.

Ion intensities are converted to absolute cross sections using a Beer's law analysis as described previously.[22] Absolute uncertainties in the cross section magnitudes are estimated to be ±20%, which are largely the result of errors in the pressure measurement and length of the interaction region. Relative uncertainties are approximately ±5%.

Ion kinetic energies in the laboratory frame, E_{lab}, are converted to energies in the center-of-mass frame, E_{CM}, using the formula $E_{CM} = E_{lab}m/(m + M)$, where M and m are the masses of the ionic and neutral reactants, respectively. All energies reported here are in the CM frame unless otherwise noted. The absolute zero and distribution of the ion kinetic energies are determined using the octopole ion guide as a retarding potential analyzer as previously described.[22] The distribution of ion kinetic energies is nearly Gaussian with a full width at half-maximum (fwhm) between 0.3 and 0.7 eV (lab) for these experiments. The uncertainty in the absolute energy scale is ±0.05 eV (lab).

Pressure-dependent studies of all systems examined here were performed because the threshold regions of the CID cross sections are sensitive to the effects of multiple collisions. Data free from pressure effects are obtained by extrapolating to zero pressure of the Xe reactant, as described previously.[23] CID cross sections subjected to thermochemical analysis are therefore the result of single bimolecular encounters.

Theoretical Calculations. To obtain model structures, vibrational frequencies, rotational constants, and energetics for the ionized $(N\text{-L})^+$ ligands and $Zn^+(N\text{-L})_x$ complexes, density functional theory calculations were performed using the Gaussian 98 and Gaussian 03 suites of programs.[24] While experiments were only performed for the $Zn^+(4,4'\text{-dipyridyl})_x$ complexes, where x = 1−3, calculations were also performed for x = 4. Similarly, experiments were only performed for the mono- and bis complexes of 2,2′-dipyridyl and 1,10-phenanthroline, but calculations were also performed for the tris complexes to these ligands. The neutral (*N*-L) ligands and the transition state (TS) for the interconversion of *cis*- and *trans*-2,2′-dipyridyl were calculated in our previous work.[1] In the present study, we also calculate the potential energy surface (PES) for the interaction of Zn^+ with 2,2′-dipyridyl and the interconversion of the Zn^+ bound cis and trans conformers of 2,2′-dipyridyl. Geometry optimizations and frequency analyses were performed at the B3LYP/6-31G* level.[25,26] When used to model the data or to calculate thermal energy corrections, the B3LYP/6-31G* vibrational frequencies are prescaled by a factor of 0.9804.[27] The prescaled vibrational frequencies thus obtained for these systems are listed in Table 1S in the Supporting Information, while Table 2S in the Supporting Information lists the rotational constants. Single point energy

calculations were performed at the B3LYP/6-311+G(2d,2p) and M06/6-311+G(2d,2p) levels of theory using the B3LYP/6-31G* optimized geometries. Independent zero point energy (ZPE) and basis set superposition error (BSSE) corrections are included in the calculated BDEs.[28,29]

Thermochemical Analysis. The threshold regions of the CID cross sections are modeled using eq 1:

$$\sigma(E) = \sigma_0 \sum_i g_i (E + E_i - E_0)^n / E \quad (1)$$

where σ_0 is an energy independent scaling factor, E is the relative translational energy of the reactants, E_0 is the threshold for reaction of the ground electronic and ro-vibrational states, and n is an adjustable parameter that describes the efficiency of kinetic to internal energy transfer.[30] The summation is over the ro-vibrational states of the reactant ions, i, where E_i is the excitation energy of each state and g_i is the population of those states ($\sum g_i = 1$). The relative reactivity of all ro-vibrational states, as reflected by σ_0 and n, is assumed to be equivalent.

The density of ro-vibrational states is determined using the Beyer–Swinehart algorithm,[31,32] and the relative populations, g_i, are calculated for a Maxwell–Boltzmann distribution at 298 K, the internal temperature of the reactants. The vibrational frequencies and rotational constants are derived from electronic structure calculations as described in the Theoretical Calculations section. We have scaled the vibrational frequencies by ±10% to encompass the range of average scaling factors needed to achieve agreement with experimentally determined frequencies.[33] The corresponding change in the average vibrational energy is taken to be an estimate of one standard deviation of the uncertainty in the vibrational energy (Table 1S in the Supporting Information).

We also consider the possibility that collisionally activated ions do not dissociate on the time scale of our experiment (~100 μs) by including statistical theories for unimolecular dissociation, specifically Rice–Ramsperger–Kassel–Marcus (RRKM) theory, into eq 1 as described in detail elsewhere.[16,34] The ro-vibrational frequencies appropriate for the energized molecules (EMs) and the TSs leading to dissociation are given in Tables 1S and 2S in the Supporting Information. We assume that the TSs are loose and productlike because the interaction between Zn^+ and the (N-L) ligands is largely electrostatic. Therefore, the TS vibrations used are the frequencies corresponding to the products, which are also found in Table 1S in the Supporting Information. The transitional frequencies, those that become rotations and translations of the completely dissociated products, are treated as rotors, a treatment that corresponds to a phase space limit (PSL) and is described in detail elsewhere.[16]

The model represented by eq 1 is expected to be appropriate for translationally driven reactions[35] and has been found to reproduce CID cross sections well. The model is convoluted with the kinetic energy distributions of both the reactant $Zn^+(N\text{-L})_x$ complex and neutral Xe atom, and a nonlinear least-squares analysis of the data is performed to give optimized values for the parameters σ_0, E_0, and n. The error associated with the measurement of E_0 is estimated from the range of threshold values determined for the zero-pressure-extrapolated data sets, variations associated with uncertainties in the vibrational frequencies (±10% scaling as discussed above), and the uncertainty in the absolute energy scale, ± 0.05 eV (lab). For analyses that include RRKM lifetime effects, the uncertainties in the reported E_0(PSL) values also include the effects of increasing and decreasing the time assumed available for dissociation by a factor of 2.

Equation 1 explicitly includes the internal energy of the ion, E_i. All energy available is treated statistically because the ro-vibrational energy of the reactants is redistributed throughout the $Zn^+(N\text{-L})_x$ complex upon impact with the Xe atom. The threshold energies, E_0(PSL), obtained from these analyses can be equated to 0 K BDEs because the CID processes examined here are simple noncovalent bond cleavage reactions.[23,36]

In the CID of the Zn^+(pyridine) and Zn^+(4,4′-dipyridyl) complexes, two low-energy dissociation pathways occur in parallel: loss of a neutral zinc atom to produce the ionized ligand, $(N\text{-L})^+$, and loss of the neutral ligand, (N-L), to produce Zn^+. These two pathways may compete with each other. To properly account for competitive effects and extract accurate threshold energies from these experimental cross sections, the statistical model of eq 1 is modified to incorporate the competition between the various dissociation pathways as shown in eq 2 and described in detail previously.[37]

$$\sigma_j(E) = \frac{n\sigma_{0,j}}{E} \sum_i g_i \int_0^{E+E_i-E_0} \frac{k_j(E^*)}{k_{tot}(E^*)} \times [1 - e^{-k_{tot}(E^*)\tau}](\Delta E)^{n-1}\, d(\Delta E) \quad (2)$$

where most of the parameters are the same as in eq 1; τ is the experimental time available for dissociation, σ_j is the cross section for reaction channel j, k_j is the RRKM rate constant for that channel, and $k_{tot} = \sum k_j$ is the total unimolecular dissociation rate constant. The ratio of the unimolecular dissociation rate constants, k_j/k_{tot}, introduces the coupling between product channels j. The term ΔE is the energy that remains in translation after the collision between the $Zn^+(N\text{-L})_x$ complex and Xe atom; hence the internal energy of the $Zn^+(N\text{-L})_x$ complex after the collision is $E^* = E + E_i - \Delta E$. $\sigma_{0,j}$ is an energy independent scaling factor for the j^{th} dissociation channel, which in principle should be the same for all channels. However, empirically imposing this constraint does not allow all of the data to be reproduced with high fidelity.

RESULTS

Cross Sections for Collision-Induced Dissociation. Experimental cross sections were obtained for the interaction of Xe with 11 $Zn^+(N\text{-L})_x$ complexes, where (N-L) = pyridine and x = 1–4, 4,4′-dipyridyl and x = 1–3, 2,2′-dipyridyl and x = 1–2, and 1,10-phenanthroline and x = 1–2. Figure 2 shows representative data for the interaction of Xe with the Zn^+(2,2′-dipyridyl)$_x$ complexes. CID data for the other $Zn^+(N\text{-L})_x$ complexes are shown in the Supporting Information as Figure 1S. The most favorable process for the monoligated $Zn^+(N\text{-L})$ complexes is loss of a neutral Zn atom to produce the ionized ligand, $(N\text{-L})^+$, in the CID reactions 3.

$$Zn^+(N\text{-L}) + Xe \rightarrow Zn + (N\text{-L})^+ + Xe \quad (3)$$

At elevated energies activated dissociation of the ionized ligand resulting in loss of one or two molecules of HCN is also observed for the complexes to 4,4′-dipyridyl, 2,2′-dipyridyl, and 1,10-phenanthroline. In contrast, the most favorable processes for the $Zn^+(N\text{-L})_x$ complexes, where $x > 1$, is loss of an intact neutral ligand in the CID reactions 4.

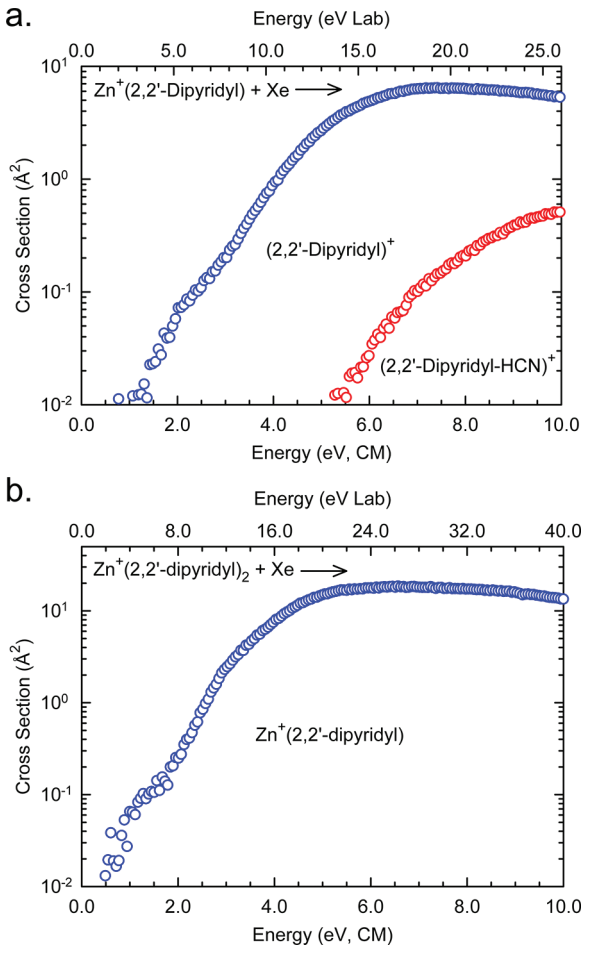

Figure 2. Cross sections for CID of $Zn^+(2,2'\text{-dipyridyl})_x$ complexes, where $x = 1$ and 2, parts a and b, respectively, with Xe as a function of kinetic energy in the center-of-mass frame (lower x-axis) and laboratory frame (upper x-axis). Data are shown for a Xe pressure of ~0.2 mTorr.

$$Zn^+(N\text{-}L)_x + Xe \rightarrow Zn^+(N\text{-}L)_{x-1} + (N\text{-}L) + Xe \quad (4)$$

Reaction 4 also occurs for the Zn^+(pyridine) and Zn^+(4,4′-dipyridyl) complexes, but exhibits a larger apparent threshold and smaller cross section than the ionized ligand of reaction 3. At elevated energies dissociation of additional neutral (N-L) or ionized $(N\text{-}L)^+$ ligands is observed for the $Zn^+(N\text{-}L)_x$ complexes where $x > 1$. The shapes of the CID cross sections confirm that these products are formed sequentially from the primary $Zn^+(N\text{-}L)_{x-1}$ product. Ligand exchange to produce Zn^+Xe is only observed as a minor reaction pathway in the CID of Zn^+(pyridine).

Threshold Analysis. The model of eq 1 was used to analyze the threshold regions for reaction 4 in nine $Zn^+(N\text{-}L)_x$ complexes (i.e., all complexes except Zn^+(2,2′-dipyridyl) and Zn^+(1,10-phenanthroline)), thereby allowing the direct determination of the $(N\text{-}L)_{x-1}Zn^+\text{–}(N\text{-}L)$ BDEs. For the monoligated $Zn^+(N\text{-}L)$ complexes, the model of eq 1 was used to analyze the thresholds for reaction 3, corresponding to the $(N\text{-}L)^+$ product cross section, and thereby providing the $Zn\text{–}(N\text{-}L)^+$ BDEs. The $Zn^+\text{–}(N\text{-}L)$ BDEs were then determined using the thermochemical cycles of eq 5 and the measured ionization energies (IEs) of Zn and the (N-L) ligands.[38]

$$D_0[Zn^+ - (N\text{-}L)] = D_0[Zn - (N\text{-}L)^+] + IE[Zn] - IE[(N\text{-}L)] \quad (5)$$

For the Zn^+(pyridine) and Zn^+(4,4′-dipyridyl) complexes the cross sections for reactions 3 and 4 were also analyzed competitively using the model of eq 2. The competitive data analyses are believed to provide the most accurate assessment of the thermodynamic thresholds for CID of the $Zn^+(N\text{-}L)$ complexes, while comparison to the results obtained for the independent analyses allow the competitive shifts to be assessed. Sequential dissociation processes lead to a high-energy falloff in the primary product cross section for the

Table 1. Fitting Parameters of eq 1, Threshold Dissociation Energies at 0 K, and Entropies of Activation at 1000 K of $Zn^+(N\text{-}L)_x$ Complexes[a]

species	$\sigma_0{}^b$	n^b	$E_0{}^c$ (eV)	$E_0(PSL)^b$ (eV)	kinetic shift (eV)	$\Delta S^{\ddagger}(PSL)^b$ (Jmol^{-1}K^{-1})
Zn^+(pyridine)	5.5 (0.2)	0.9 (0.1)	2.81 (0.03)	2.53 (0.07)	0.28	34.1 (2.0)
	27.7 (0.5)[d]	0.9 (0.1)[d]	2.60 (0.03)[d]	2.37 (0.07)[d]	0.23[d]	42.2 (2.0)[d]
	9.5 (0.4)[e]	1.2 (0.1)[e]	–	2.48 (0.04)[e]	–	34.7 (2.0)[e]
	26.5 (0.1)[f]	1.2 (0.1)[f]	–	2.30 (0.03)[f]	–	42.1 (2.0)[f]
$Zn^+(pyridine)_2$	15.7 (0.4)	0.8 (0.1)	1.85 (0.03)	1.61 (0.04)	0.24	37.8 (4.4)
$Zn^+(pyridine)_3$	42.1 (1.9)[g]	0.9 (0.1)[g]	1.31 (0.06)[g]	1.06 (0.04)[g]	0.25[g]	37.2 (4.5)[g]
$Zn^+(pyridine)_4$	107.7 (4.0)[g]	1.0 (0.1)[g]	0.99 (0.07)[g]	0.79 (0.02)[g]	0.20[g]	92.5 (5.0)[g]
Zn^+(4,4-dipyridyl)	0.2 (0.1)	1.2 (0.1)	4.07 (0.11)	2.59 (0.09)	1.48	31.9 (2.0)
	5.7 (0.5)[d]	1.0 (0.1)[d]	3.42 (0.07)[d]	2.35 (0.07)[d]	1.07[d]	41.7 (1.7)[d]
	5.6 (0.4)[e]	1.0 (0.1)[e]	–	2.58 (0.08)[e]	–	32.0 (2.0)[e]
	5.6 (0.4)[f]	1.0 (0.1)[f]	–	2.35 (0.08)[f]	–	41.8 (2.0)[f]
$Zn^+(4,4\text{-dipyridyl})_2$	13.9 (3.0)	0.9 (0.1)	2.51 (0.16)	1.56 (0.07)	0.95	47.5 (4.3)
$Zn^+(4,4\text{-dipyridyl})_3$	23.2 (3.1)[g]	1.2 (0.1)[g]	1.74 (0.10)[g]	0.76 (0.04)[g]	0.98[g]	67.1 (4.2)[g]
Zn^+(2,2-dipyridyl)	2.9 (0.9)[e]	1.8 (0.2)[e]	4.51 (0.10)[e]	2.57 (0.10)[e]	1.94[e]	62.1 (1.8)[e]
$Zn^+(2,2\text{-dipyridyl})_2$	36.5 (9.8)	1.0 (0.3)	4.20 (0.19)	2.34 (0.13)	1.86	86.8 (4.6)
Zn^+(1,10-phenanthroline)	102.8 (8.7)[e]	0.9 (0.1)[e]	5.59 (0.08)[e]	3.00 (0.11)[e]	2.59[e]	67.9 (1.8)[e]
$Zn^+(1,10\text{-phenanthroline})_2$	32.8 (2.0)	1.3 (0.1)	4.89 (0.06)	2.46 (0.10)	2.43	83.6 (4.6)

[a]Uncertainties are listed in parentheses. [b]Average values for loose PSL transition state. [c]No RRKM analysis. [d]Average values obtained for fits to the ionized N-donor ligand, $(N\text{-}L)^+$. [e]Average values obtained from competitive fitting for the Zn^+ channel. [f]Average values obtained from competitive fitting for the ionized N-donor ligand, $(N\text{-}L)^+$. [g]Average values obtained for fits to the total cross section.

dx.doi.org/10.1021/jp207144b | J. Phys. Chem. A 2012, 116, 1319–1332

$Zn^+(N\text{-}L)_x$ complexes, where x = 3 and 4, that is not appropriately handled by eq 1. Thus, analyses of the total CID cross sections were performed for these large complexes.

Results of these analyses are provided in Table 1. Good reproduction of the data is obtained over energy ranges exceeding 5.0 eV for all $Zn^+(N\text{-}L)_x$ complexes except $Zn^+(pyridine)_4$, where the reproduction of data is limited to ~3 eV. The zero-pressure-extrapolated CID cross sections and fits to the data using a loose PSL model for the interaction of $Zn^+(2,2'\text{-dipyridyl})_x$, where x = 1 and 2, with Xe are shown in Figure 3. Threshold analyses of the other $Zn^+(N\text{-}L)_x$ complexes

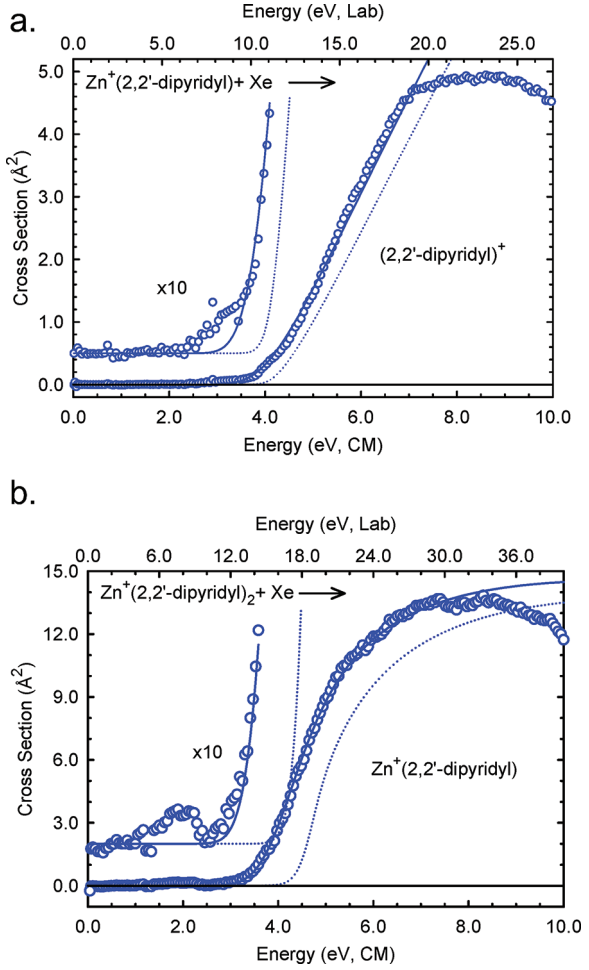

Figure 3. Zero-pressure-extrapolated cross sections for CID of $Zn^+(2,2'\text{-dipyridyl})_x$ complexes, where x = 1 and 2, parts a and b, respectively, with Xe as a function of kinetic energy in the center-of-mass frame (lower x-axis) and laboratory frame (upper x-axis). The solid lines show the best fits to the data using eq 1 convoluted over the ion kinetic and internal energy distributions. Dashed lines show the model cross section in the absence of experimental kinetic energy broadening for reactants with an internal energy corresponding to 0 K.

are shown in the Supporting Information, Figure 2S. In all cases, the cross sections are accurately reproduced using a loose PSL TS model. Previous work has shown that this model provides the most accurate assessment of the kinetic shifts for CID processes of electrostatically bound ion−molecule complexes.[39−41]

Kinetic Shifts. Two threshold values, E_0 and E_0(PSL), are listed in Table 1 for the independent analyses of the $Zn^+(N\text{-}L)_{x-1}$ and $(N\text{-}L)^+$ product cross sections for each complex. E_0 represents the threshold obtained for analyses that do not include RRKM lifetime effects, while E_0(PSL) represents the threshold obtained when the RRKM lifetime analysis is included. The difference in the E_0 and E_0(PSL) thresholds provides a measure of the kinetic shift associated with the finite time scale of our measurements. The total number of heavy atoms and vibrational modes increases as the size of the complex increases. Therefore, the density of states of the dissociating complex increases with size. The density of states also increases with energy. Thus, the observed kinetic shifts should directly correlate with the size of the complex and the threshold energy. However, the strength of binding decreases with the extent of ligation. As a result, these effects nearly cancel. The observed kinetic shifts decrease slightly with the size of the complex for a given (N-L) ligand. The kinetic shifts are much smaller for the complexes to the monodentate ligands than the chelating ligands and increase with the size of the (N-L) ligand such that they parallel the strength of the binding and follow the order $Zn^+(pyridine)_x$ < $Zn^+(4,4'\text{-dipyridyl})_x$ < $Zn^+(2,2'\text{-dipyridyl})_x$ < $Zn^+(1,10\text{-phenanthroline})_x$.

Entropies of Activation. The entropies of activation, $\Delta S^{\ddagger}$, provide a measure of the looseness (or tightness) of the TS, but are also a reflection of the complexity of the system. Listed in Table 1, the $\Delta S^{\ddagger}$(PSL) values at 1000 K vary between 32 and 94 J K^{-1} mol^{-1} for the $Zn^+(N\text{-}L)_x$ complexes examined here. The entropies increase with the size of the complex for a given (N-L) ligand, and for a fixed value of x as the size of the (N-L) ligand increases. $\Delta S^{\ddagger}$ is also larger for the chelating ligands than for the monodentate ligands as a result of the stronger and more geometrically constrained binding in the former complexes. The entropies of activation of these complexes compare favorably to a wide variety of noncovalently bound complexes previously measured in our laboratory.[1,2,16,17,37,39−41,45−48]

Theoretical Results. Theoretical structures for the ionized $(N\text{-}L)^+$ ligands and $Zn^+(N\text{-}L)_x$ complexes were calculated using Gaussian 98 and Gaussian 03 as described in the Theoretical Calculations section. Key geometrical parameters of the B3LYP/6-31G* optimized structures for each of these species are summarized in Table 2. Table 3 provides the calculated BDEs determined at the B3LYP/6-311+G(2d,2p) and M06/6-311+G(2d,2p) levels of theory using the B3LYP/6-31G* optimized structures. Independent ZPE and BSSE corrections are provided for the reported BDEs.

Neutral (N-L) Ligands. This work is a follow-up to earlier studies where we examined the analogous $Cu^+(N\text{-}L)_x$ and $Ni^+(N\text{-}L)_x$ systems.[1,2] As this work involves the same N-donor ligands, only a brief summary of the theoretical results for these neutral ligands is given here. The B3LYP/6-31G* optimized structures of the neutral (N-L) ligands along with their measured and calculated dipole moments and isotropic molecular polarizabilities are shown in Figure 1.[1,15,42−44] The ground-state structures of pyridine, *trans*-2,2′-dipyridyl, and 1,10-phenanthroline are planar, while the aromatic rings of 4,4′-dipyridyl and *cis*-2,2′-dipyridyl are twisted relative to each other. The dipole moment of pyridine is measured as 2.215 ± 0.010 D[15] and calculated to be 2.31 D. 2,2′-Dipyridyl and 4,4′-dipyridyl exhibit no net dipole moment because the local dipole moments cancel as a result of the symmetry of these ligands. However, the local dipoles reinforce to produce a large dipole moment in the cis conformer, 3.04 D. 1,10-Phenanthroline has the largest dipole moment among these ligands, 3.31 D, due to the more extensive π network. Pyridine has the smallest

Table 2. Geometrical Parameters of the B3LYP/6-31G* Optimized Structures of the Neutral and Ionized $(N\text{-L})^+$ Ligands and $Zn^+(N\text{-L})_x$ Complexes[a]

species	bond length (Å)	bond angle (deg)		
	Zn^+–N	∠NCCN	∠CCCC	∠NZn$^+$N
Zn^+(pyridine)	1.971			
Zn^+(pyridine)$_2$	2.039 (2)			106.2
Zn^+(pyridine)$_3$	2.083 (3)			104.8 (3)
Zn^+(pyridine)$_4$	2.013 (4)			105.4
				108.9 (3)
				112.3 (2)
4,4′-dipyridyl			36.2	
4,4′-dipyridyl$^+$			48.7	
Zn^+(4,4′-dipyridyl)	1.962		32.5	
Zn^+(4,4′-dipyridyl)$_2$	2.033 (2)		34.0 (2)	105.9
Zn^+(4,4′-dipyridyl)$_3$	2.054 (3)		33.4 (3)	107.2 (3)
Zn^+(4,4′-dipyridyl)$_4$	2.007 (4)		32.3 (4)	105.9
				108.9 (3)
				112.1 (2)
trans-2,2′-dipyridyl		180.0		
cis-2,2′-dipyridyl		35.1		
trans-2,2′-dipyridyl$^+$		180.0		
cis-2,2′-dipyridyl$^+$		0.0		
Zn^+(2,2′-dipyridyl)	2.044 (2)	0.3		81.5
Zn^+(2,2′-dipyridyl)$_2$	2.000 (4)	4.9 (2)		83.7 (2)
				117.1 (2)
				130.6 (2)
Zn^+(2,2′-dipyridyl)$_3$	2.149 (2)	8.6 (3)	9.4 (3)	75.3
	2.188 (4)			93.2 (3)
				95.8 (8)
				168.3 (3)
1,10-phenanthroline		0.0		
1,10-phenanthroline$^+$		0.0		
Zn^+(1,10-phenanthroline)	2.057 (2)	0.0		82.7
Zn^+(1,10-phenanthroline)$_2$	2.010 (4)	0.0		84.7 (2)
				116.4 (2)
				130.4 (2)
Zn^+(1,10-phenanthroline)$_3$	2.168 (4)	2.0 (3)		77.1 (3)
	2.213 (2)			93.8 (3)
				95.1 (6)
				168.6 (3)

[a]Average values are given for similar bond distances or angles; degeneracies are listed in parentheses.

polarizability among these ligands (9.25 ± 0.15 Å^3 measured,[15] 9.27 Å^3 calculated). The calculated polarizabilities of 4,4′-dipyridyl, *cis*-2,2′-dipyridyl, and *trans*-2,2′-dipyridyl are similar, 19.32, 19.67, and 19.92 Å^3, respectively, slightly more than twice that of pyridine. The polarizability of 1,10-phenanthroline is the largest, 23.78 Å^3, in accord with its being the largest of these (*N*-L) ligands.

The theoretical calculations find that, in all of the $Zn^+(N\text{-L})_x$ complexes, Zn^+ prefers to bind to the lone pair(s) of electrons on the nitrogen atom(s) rather than to the π cloud of the aromatic ring(s). This preference for metal cation binding to the lone pair of electrons on the nitrogen atom(s) over binding to the π cloud was previously observed for a wide variety of metal ion-(*N*-L) ligand complexes.[1,2,40,45−49]

Zn^+(pyridine)$_x$. The ground-state structures of the Zn^+(pyridine)$_x$ complexes optimized at the B3LYP/6-31G* level of theory are shown in Figure 4. The arrangement of the N donor atoms of the pyridine ligands around Zn^+ approaches the ideal structures predicted by the valence shell electron pair repulsion (VSEPR) model[49] for the Zn^+(pyridine)$_x$ complexes, where x = 1−3 in which the valence 4s electron of Zn^+ interacts repulsively with the pyridine ligands, i.e., linear for x = 1, bent for x = 2, and trigonal pyramidal for x = 3. However, the effects of the valence 4s electron on the geometry of the Zn^+(pyridine)$_4$ complex appear to wash out as the arrangement of the N donor atoms around Zn^+ is only slightly distorted from an ideal tetrahedral geometry. This behavior may arise because the Zn^+(pyridine)$_4$ complex is formally a 19-electron species.

In the Zn^+(pyridine) complex, the Zn^+–N bond length is 1.971 Å and increases to 2.039 Å in the Zn^+(pyridine)$_2$ complex. The ground-state structure of Zn^+(pyridine)$_2$ is bent, and the two pyridine rings are twisted relative to each other. The ∠NZn$^+$N of the Zn^+(pyridine)$_2$ complex is 104.8° to minimize the repulsive interactions between the two pyridine rings and the 4s electron of the Zn^+ cation. Interaction of three pyridine ligands with Zn^+ adopts a trigonal pyramidal conformation with three similar Zn^+–N bond lengths of 2.083 Å and three similar ∠NZn$^+$N bond angles of 104.8°, and the pyridine rings are twisted with respect to each other to minimize ligand−ligand and ligand−Zn 4s electron repulsive interactions. With four pyridine ligands, the optimized structure is found to exhibit a slightly distorted tetrahedral arrangement of the pyridine ligands around the zinc ion. The Zn^+–N bond lengths are similar, 2.013 Å, and shorter than in the bis and tris complexes.

Zn^+(4,4′-dipyridyl)$_x$. The B3LYP/6-31G* ground-state structures of the Zn^+(4,4′-dipyridyl)$_x$ complexes are shown in Figure 3S of the Supporting Information. The binding geometries found are similar to those computed for the Zn^+(pyridine)$_x$ complexes. In neutral 4,4′-dipyridyl, the pyridyl moieties are twisted with respect to each other by 36.2° to minimize repulsion between the H6 and H6′ atoms of the adjacent pyridyl rings. Upon binding to Zn^+, the dihedral angle between the two pyridyl moieties reduces to 32.5° as a result of donation of electron density to Zn^+. The dihedral angle between the two pyridyl moieties of the 4,4′-dipyridyl ligands is not significantly altered by further ligation (Table 3). The Zn^+–N bond lengths are very similar to those in the Zn^+(pyridine)$_x$ complexes and increase from 1.962 to 2.054 Å as the number of 4,4′-dipyridyl ligands bound to Zn^+ increases from one to three as a result of increasing ligand−ligand repulsion. As found for the Zn^+(pyridine)$_x$ complexes, the Zn^+–N bond lengths in the Zn^+(4,4′-dipyridyl)$_4$ complex are slightly shorter than those of the Zn^+(4,4′-dipyridyl)$_3$ complex, 2.007 vs 2.054 Å, respectively.

Zn^+(2,2′-dipyridyl)$_x$. The B3LYP/6-31G* ground-state structures of the Zn^+(2,2′-dipyridyl)$_x$ complexes are shown in Figure 5. In the ground-state conformation of neutral 2,2′-dipyridyl, the two pyridyl rings are coplanar and the two nitrogen atoms are located on opposite sides of the central C–C bond, i.e., the trans conformer shown in Figure 1. However, complexation of 2,2′-dipyridyl to Zn^+ is much stronger when the pyridyl rings rotate through the central C–C bond to orient both N atoms so that they may simultaneously interact with the Zn^+ ion. The ∠NCCN dihedral angle of neutral *trans*-2,2′-dipyridyl is 180°, and

dx.doi.org/10.1021/jp207144b | J. Phys. Chem. A 2012, 116, 1319−1332

Table 3. Bond Dissociation Energies of $Zn^+(N\text{-}L)_x$ Complexes at 0 K in kJ/mol

		theory			
	experiment	M06		B3LYP	
complex	TCID[a]	D_0[c]	$D_{0,BSSE}$[d]	D_0[e]	$D_{0,BSSE}$[d]
Zn^+(pyridine)	239.7 (3.6)	232.7	230.1	235.0	233.1
	246.9 (6.9)[b]				
$Zn^+(pyridine)_2$	154.8 (4.3)	130.5	126.7	121.2	119.3
$Zn^+(pyridine)_3$	102.2 (3.8)	97.7	94.6	77.0	74.6
$Zn^+(pyridine)_4$	76.1 (2.0)	97.1	92.4o	65.7	64.6
Zn^+(4,4′-dipyridyl)	248.8 (8.8)	238.3	235.7	236.8	234.9
$Zn^+(4,4'\text{-dipyridyl})_2$	150.2 (6.9)	129.3	126.9	116.4	114.4
$Zn^+(4,4'\text{-dipyridyl})_3$	73.3 (4.0)	94.3	91.1	65.9	63.3
$Zn^+(4,4'\text{-dipyridyl})_4$	–	117.9	113.4	39.9	36.5
Zn^+(2,2′-dipyridyl)	348.8 (10.1)	357.0	353.2	335.5	332.5
$Zn^+(2,2'\text{-dipyridyl})_2$	225.2 (13.1)	257.2	252.1	206.3	201.9
$Zn^+(2,2'\text{-dipyridyl})_3$	–	135.7	129.8	56.3	49.2
Zn^+(1,10-phenanthroline)	395.1 (5.4)	360.0	356.2	365.2	362.2
$Zn^+(1,10\text{-phenanthroline})_2$	236.8 (10.2)	251.2	246.2	227.9	223.7
$Zn^+(1,10\text{-phenanthroline})_3$	–	142.7	135.2	89.8	82.6
AEU/MAD	6.6 (3.5)	18.1 (10.1)	17.8 (10.5)	18.1 (10.5)	20.6 (10.8)

[a]Present results except as noted, threshold collision-induced dissociation (TCID). [b]Reference 44. [c]Calculated at the M06/6-311+G(2d,2p) level of theory using B3LYP/6-31G* optimized geometries including ZPE corrections with B3LYP/6-31G* frequencies scaled by 0.9804. [d]Also includes BSSE corrections. [e]Calculated at the B3LYP/6-311+G(2d,2p) level of theory using B3LYP/6-31G* optimized geometries including ZPE corrections with B3LYP/6-31G* frequencies scaled by 0.9804.

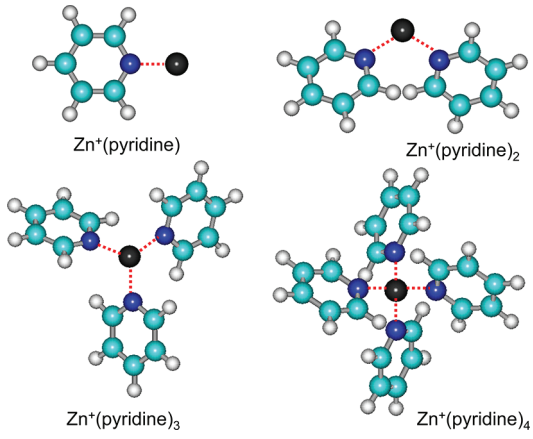

Figure 4. B3LYP/6-31G* optimized geometries of $Zn^+(pyridine)_x$ complexes, where x = 1−4.

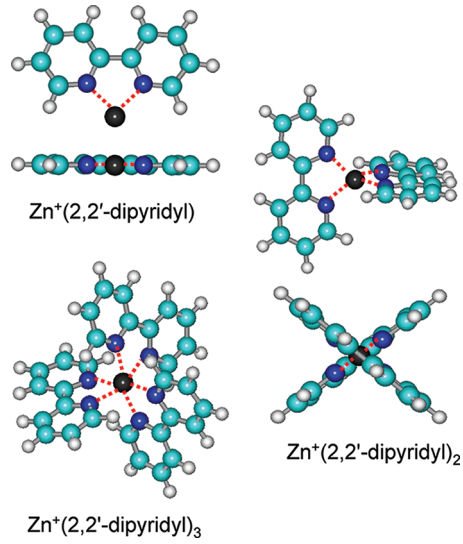

Figure 5. B3LYP/6-31G* optimized geometries of $Zn^+(2,2'\text{-dipyridyl})_x$ complexes, where x = 1−3.

reduces to 35.1° in the cis conformation. Upon complexation of *trans*-2,2′-dipyridyl with Zn^+, the ∠NCCN dihedral angle reduces from 180 to 0.3°. The ∠NCCN dihedral angle increases slightly with ligation as a result of ligand−ligand repulsive interactions. The Zn^+−N bond distances in the $Zn^+(2,2'\text{-dipyridyl})_x$ complexes vary, and are 2.044, 2.000, and 2.149 Å for x = 1, 2, and 3, respectively. The Zn^+−N bond lengths are again the shortest when Zn^+ binds to four N atoms. The $Zn^+(2,2'\text{-dipyridyl})_2$ complex exhibits a distorted tetrahedral arrangement of the N atoms around Zn^+, and the two dipyridyl ligands are oriented with an angle of 80.9° to achieve the maximum binding interaction and minimize ligand−ligand repulsion. The $Zn^+(2,2'\text{-dipyridyl})_3$ complex exhibits a distorted octahedral geometry where all three ligands have ∠NCCN dihedral angles of 8.6° (Table 2).

$Zn^+(1,10\text{-phenanthroline})_x$. The B3LYP/6-31G* ground-state structures of the $Zn^+(1,10\text{-phenanthroline})_x$ complexes are shown in Figure 6. The optimized geometry of the $Zn^+(1,10\text{-phenanthroline})$ complex is similar to that observed for $Zn^+(2,2'\text{-dipyridyl})$ except that the Zn^+−N bond lengths are slightly longer, 2.057 vs 2.044 Å. The 1,10-phenanthroline ligand remains planar upon complexation with Zn^+. The $Zn^+(1,10\text{-phenanthroline})_2$ complex exhibits a distorted tetrahedral arrangement of N atoms around Zn^+, and the two 1,10-phenanthroline molecules are oriented at an angle of 100.4° with respect to each other. The $Zn^+(1,10\text{-phenanthroline})_3$ complex exhibits a distorted octahedral arrangement of N atoms around Zn^+ similar to that of the $Zn^+(2,2'\text{-dipyridyl})_3$ complex. The significant ligand−ligand repulsion results in distortion of the planar geometry of the 1,10-phenanthroline ligands such that the ∠NCCN dihedral angle increases to 2.0°.

Trends in the Zn^+−N bond lengths appear to be most closely related to the flexibility of the ligand framework, rather than the relative bond strengths. The $Zn^+(pyridine)_x$ and $Zn^+(4,4'$-

dx.doi.org/10.1021/jp207144b | J. Phys. Chem. A 2012, 116, 1319−1332

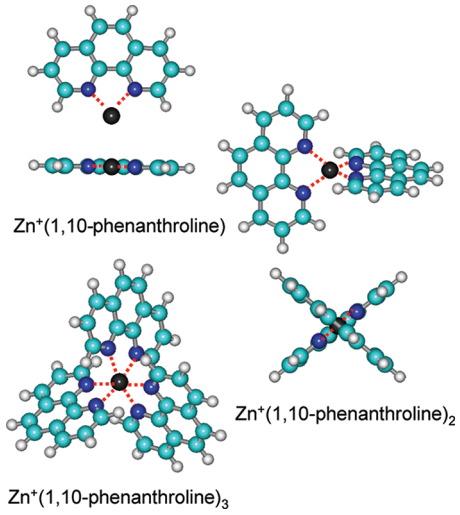

Figure 6. B3LYP/6-31G* optimized geometries of Zn^+(1,10-phenanthroline)$_x$ complexes, where x = 1−3.

dipyridyl)$_x$ complexes exhibit Zn^+−N bond lengths that are very similar and shorter than those in the Zn^+(2,2′-dipyridyl)$_x$ complexes, which are shorter than those in the Zn^+(1,10-phenanthroline)$_x$ complexes. This parallels the flexibility of these ligands and their ability to make structural changes to optimize their binding interactions. Somewhat surprisingly, all of the Zn^+(*N*-L)$_x$ complexes, with four Zn^+−N donor interactions, exhibit Zn^+−N bond lengths that are shorter than those in the smaller or larger complexes.

As shown in Figure 4 and Figure 3S in the Supporting Information, complexes of Zn^+ to the monodentate ligands exhibit bent geometries with ∠NZn$^+$N bond angles of 106° for the bis complexes and trigonal pyramidal geometries with ∠NZn$^+$N bond angles of 105° for the tris complexes. This behavior arises because the 4s electron of Zn^+ experiences repulsion with the ligands. However, interaction of Zn^+ with four monodentate ligands exhibits a distorted tetrahedral geometry with ∠NZn$^+$N bond angles of ∼108°, which suggests that ligand−ligand repulsion is the dominant factor controlling the structures of Zn^+(pyridine)$_4$ and Zn^+(4,4′-dipyridyl)$_4$, rather than the electron configuration of Zn^+. Attempts to find a stable structure exhibiting square planar or square pyramidal geometries for Zn^+(pyridine)$_4$ always converged to the energetically more favorable distorted tetrahedral geometry.

Conversion from 0 to 298 K. To allow comparison to commonly used experimental conditions, the 0 K BDEs determined here (experimentally and theoretically) are converted to 298 K bond enthalpies and free energies. The enthalpy and entropy conversions are calculated using standard formulas (assuming harmonic oscillator and rigid rotor models) and the vibrational frequencies and rotational constants determined for the B3LYP/6-31G* optimized geometries. Table 3S in the Supporting Information lists 0 and 298 K enthalpies, free energies, and enthalpic and entropic corrections for all systems studied. Uncertainties in the enthalpic and entropic corrections are determined by ±10% variation in the molecular constants, and additionally by ±50% variation in all frequencies below 150 cm^{-1}. The latter provides a conservative estimate of the computational errors in these low frequency modes and is the dominant source of the uncertainties listed.

DISCUSSION

BDEs Derived from Independent versus Competitive Analyses. The BDEs of Zn^+(pyridine) and Zn^+(4,4′-dipyridyl) are determined by independent and competitive modeling of the Zn^+ and (*N*-L)$^+$ product cross sections because in these two systems competition among reactions 3 and 4 is clearly occurring and can be expected to influence the threshold determination. However, competitive modeling of these CID pathways influences the threshold determination for reactions 3 and 4 very little, by <0.07 and 0.01 eV for Zn^+(pyridine), and 0.05 and 0.01 eV for the Zn^+(4,4′-dipyridyl) complexes, respectively. The values obtained from competitive fitting for Zn^+(pyridine) are in better agreement with theory, providing a 6.6 (7.0) vs 11.1 (11.5) kJ/mol difference in the measured and computed values for calculations using the B3LYP (M06) functional. For the Zn^+(4,4′-dipyridyl) complex, the BDEs determined from independent and competitive modeling differ by less than 1 kJ/mol, with the competitive results again providing slightly better agreement with theory. However, the value obtained from the competitive analysis is still larger than that from B3LYP (M06) theory by 14.1 (15.7) kJ/mol. The BDEs determined via competitive analyses should be more reliable and are the values used in the latter discussions.

Comparison between Theory and Experiment. The BDEs of the Zn^+(*N*-L)$_x$ complexes, where (*N*-L) = pyridine (x = 1−4), 4,4′-dipyridyl (x = 1−3), 2,2′-dipyridyl (x = 1−2), and 1,10-phenanthroline (x = 1−2) at 0 K, measured here by guided ion beam mass spectrometry are summarized in Table 3. Also listed here are 0 K BDEs calculated at the B3LYP/6-311+G(2d,2p) and M06/6-311+G(2d,2p)//B3LYP/6-31G* levels of theory, including independent ZPE and BSSE corrections. The agreement between the theoretically and experimentally determined BDEs for all 11 Zn^+(*N*-L)$_x$ complexes examined here is illustrated in Figure 7. The mean

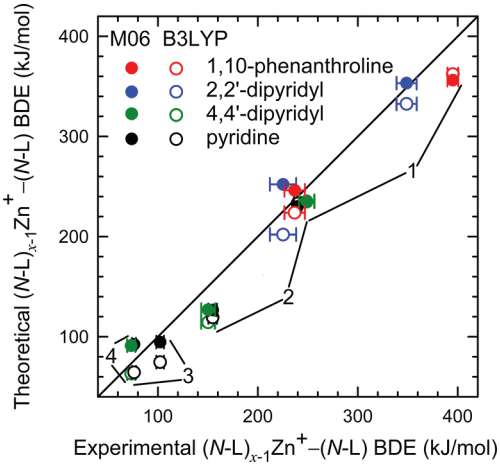

Figure 7. Theoretical versus experimental (*N*-L)$_{x-1}$Zn$^+$−(*N*-L) BDEs at 0 K (in kJ/mol), where (*N*-L) include 1,10-phenanthroline, 2,2′-dipyridyl, 4,4′-dipyridyl, and pyridine. The diagonal line indicates the values for which calculated and measured BDEs are equal.

absolute deviation (MAD) between B3LYP (M06) theory and experiment for all 11 Zn^+(*N*-L)$_x$ complexes is 20.6 ± 10.8 (17.8 ± 10.5) kJ/mol, significantly larger than the average experimental uncertainty (AEU) of 6.6 ± 3.5 kJ/mol for these complexes. When BSSE corrections are not included in the computed BDEs, the MAD improves slightly for B3LYP

dx.doi.org/10.1021/jp207144b | J. Phys. Chem. A 2012, 116, 1319−1332

theory, but degrades slightly for M06 theory, 18.1 ± 10.5 (18.1 ± 10.1) kJ/mol. In all cases, the measured BDEs exceed the B3LYP calculated BDEs. In contrast, roughly half of the BDEs slightly exceed the measured values when M06 theory is employed. Overall, these results suggest that higher levels of theory are needed to provide an accurate description of the energetics of binding in these $Zn^+(N\text{-L})_x$ complexes, and that M06 theory outperforms B3LYP. The challenge associated with accurately describing the energetics of binding in these $Zn^+(N\text{-L})_x$ complexes is not entirely clear, but likely arises because these complexes are open shell species, which are always more challenging to described than closed shell systems.

Zn^+–Pyridine BDE. Table 3 compares the present experimental results for the BDE of the Zn^+(pyridine) complex to that previously measured in our laboratory using the same threshold collision-induced dissociation (TCID) techniques employed here. The BDE for the Zn^+(pyridine) complex is determined here via independent and competitive analyses of the Zn^+ and pyridine$^+$ product cross sections. The individual analyses of the Zn^+ and pyridine$^+$ (using the thermochemical cycle of eq 5 and the measured IEs of Zn and the pyridine ligand) product cross sections provide Zn^+–pyridine BDEs of 244.2 ± 7.3 and 241.2 ± 6.9 kJ/mol, respectively. These values are in excellent agreement with the value previously determined by TCID (246.9 ± 6.9 kJ/mol). Unfortunately, in the previous study[46] the pyridine$^+$ product cross section was not collected. Therefore, the Zn^+–pyridine BDE previously determined via analysis of the Zn^+ product cross section should represent an upper limit to the BDE. The experimental BDE determined via competitive analysis of the Zn^+ and pyridine$^+$ product cross sections, 239.7 ± 3.6 kJ/mol, represents the most accurate determination of the Zn^+–pyridine BDE. This value is also in better agreement with the B3LYP and M06 calculated Zn^+–pyridine BDEs.

Relative IEs of Zn and the (*N*-L) Ligands. The ionization energies (IEs) of Zn, pyridine, and 4,4′-dipyridyl have previously been measured as 9.39420 ± 0.00002,[71] 9.26 ± 0.01,[38] and 9.10 ± 0.02 eV,[38] respectively. Thus, the relative IEs of Zn versus pyridine and 4,4′-dipyridyl are 0.13 ± 0.01 and 0.29 ± 0.01 eV, respectively. The difference in the threshold energies determined for the Zn^+ and $(N\text{-L})^+$ product cross sections from competitive analyses of the Zn^+(pyridine) and Zn^+(4,4′-dipyridyl) CID cross sections are 0.18 ± 0.05 and 0.23 ± 0.11 eV (Table 1), respectively. The relative IEs and thresholds for the CID product cross sections for these systems are within experimental error, suggesting that that the measured IEs reported in the literature and the threshold energies determined here provide accurate and reliable thermochemistry. Somewhat surprisingly, the differences in the threshold energies determined for the Zn^+ and $(N\text{-L})^+$ product cross sections from independent analyses of the Zn^+(pyridine) and Zn^+(4,4′-dipyridyl) CID cross sections are 0.16 ± 0.10 and 0.24 ± 0.11 eV (Table 1), which are also within experimental error, and in fact exhibit slightly better agreement with the reported IEs. The B3LYP calculations performed here find IEs for Zn, pyridine, and 4,4′-dipyridyl of 9.43, 9.05, and 8.81 eV, respectively. Thus, B3LYP theory suggests that the relative IEs of Zn versus pyridine and 4,4′-dipyridyl are 0.38 and 0.61 eV, respectively. These differences are larger than those found for the measured IEs and the threshold dissociation energies determined here, again suggesting that B3LYP theory is not adequately describing the energetics of these systems. Closer examination shows that the IE calculated for Zn is in excellent agreement, but that theory underestimates the IEs of pyridine and 4,4′-dipyridyl by 0.29 and 0.28 eV, respectively. The problem likely arises for the calculation of the ionized ligand, $(N\text{-L})^+$, as a result of the unpaired electron, which suggests that the BDEs determined using theory may be more reliable than the IEs as the BDEs involve calculations of the $Zn^+(N\text{-L})_x$ complexes, Zn^+, and neutral (*N*-L) ligand products.

Comparison with Literature Values. The binding energies of Zn^+ to several other ligands have previously been examined by the same energy-resolved CID techniques employed here. The Zn^+–ligand BDEs for carbon disulfide (CS_2),[50] pyrimidine,[40] adenine,[51] imidazole,[48] and triethyl phosphate (TEP)[52] were measured as 153.3 ± 23.1, 208.4 ± 7.4, 238.4 ± 5.6, 252.5 ± 9.7, and 261.5 ± 8.7 kJ/mol, respectively. Clearly, CS_2 is a much weaker ligand than all of the others, which is not surprising as its dipole moment (1.96 D) and polarizability (4.51 Å^3) are smaller than those of all of the other ligands. Among the *N*-donor ligands examined, the trends make sense based on the functional differences between these ligands. The presence of the second electron-withdrawing N atom in the ring of pyrimidine decreases the electron density on the N atom that interacts with Zn^+ as compared to pyridine, and thus the binding is weaker. Binding in adenine and imidazole is through the imidazolic N atom. Imidazole exhibits a larger dipole moment than pyridine and adenine, 3.67 vs 2.31 and 2.54 D, which leads to stronger binding of Zn^+ to imidazole and similar binding to pyridine and adenine. TEP binds Zn^+ the most strongly among the ligands examined thus far. The strong binding of Zn^+ by TEP is also not surprising as TEP possesses a large dipole moment (3.07 D) and the largest polarizability (16.42 Å^3) of these ligands. Indeed, the binding of Zn^+ by TEP is sufficiently strong that upon CID Zn^+ favors activation of TEP via elimination of ethene molecules over simple CID to lose the intact ligand.

Complexing Ability of the (*N*-L) Ligands. The ground-state structures of the neutral (*N*-L) ligands are shown in Figure 1 along with their calculated and measured dipole moments and isotropic molecular polarizabilities,[15] while the ground-state structures of the $Zn^+(N\text{-L})_x$ complexes are shown in Figures 4–6 and Figure 3S in the Supporting Information. The variation in the number of N donor atoms interacting with Zn^+, and the differences in the dipole moments, polarizabilities, and flexibilities of these ligands produces both geometric and energetic differences in the binding. Pyridine and 4,4′-dipyridyl are monodentate ligands that exhibit similar binding geometries and achieve nearly ideal arrangements of the N atoms around Zn^+ so as to minimize repulsion with the valence 4s electron on Zn^+ and among the ligands. Both 2,2′-dipyridyl and 1,10-phenanthroline are chelating ligands such that both N atoms simultaneously interact with Zn^+. Here the metal ion is incorporated into a relatively stable five-membered ring.

These (*N*-L) ligands are both strong σ donors and weak π acceptors. The lone pairs of electrons on the N atoms donate their electron density to Zn^+ and form comparatively strong dative σ bonds. The occupied orbitals of Zn^+ having the appropriate symmetry may donate electron density to the unoccupied orbitals of the (*N*-L) ligands. Both binding interactions act synergistically to produce relatively strong binding of these (*N*-L) ligands to Zn^+.

Complexation of 2,2′-dipyridyl by Zn^+ forces the two N atoms to orient themselves to simultaneously interact with the metal ion. In previous work, we computed the potential energy landscape for the conversion of *trans*-2,2′-dipyridyl into *cis*-2,2′-

dipyridyl. The energy barrier for this isomerization at 0 K is 28.9 kJ/mol relative to the ground-state trans isomer.[1] The potential energy landscape for the conversion of monodentate Zn^+(*trans*-2,2′-dipyridyl) into bidentate Zn^+(*cis*-2,2′-dipyridyl) is shown in Figure 4S of the Supporting Information. The energy barrier calculated for this isomerization at 0 K is quite small, 8.0 kJ/mol relative to the trans confomer, and is easily overcome by the energy provided by complexation. Upon complexation to Zn^+, the 2,2′-dipyridyl ligand becomes nearly planar such that the ligand experiences repulsive interactions between the H6 and H6′ atoms of the two pyridyl rings. The conjugated π system of 1,10-phenanthroline constrains this ligand to a planar geometry.

The complexing ability of Zn^+ to these (*N*-L) ligands is greatly influenced by the polarizabilities and the dipole moments of the ligands. The polarizability determines the strength of the ion−induced dipole attraction, which makes a significant contribution to the overall binding. The calculated polarizabilities of pyridine and 4,4′-dipyridyl are 9.21 and 19.32 Å^3, respectively. Metal ion binding to these ligands is fairly similar such that binding occurs with the lone pair of electrons of a single nitrogen atom. Therefore, the ion−induced dipole interaction should result in slightly stronger binding in the Zn^+(4,4′-dipyridyl) complex as compared to the Zn^+(pyridine) complex, consistent with our experimental observations. The sum of the polarizabilities of two pyridine ligands, 18.54 Å^3, is smaller than the polarizabilities of 2,2′-dipyridyl and 1,10-phenanthroline. However, the sum of the first two BDEs of $Zn^+(pyridine)_2$ is larger than the BDE for binding of the first ligand of 2,2′-dipyridyl to Zn^+ and similar to the BDE of 1,10-phenanthroline to Zn^+. This suggests that the enhanced polarizability of 2,2′-dipyridyl is insufficient to overcome the steric limitations on the binding induced by the constrained geometry and repulsive interactions between the H6 and H6′ atoms of this ligand. The similar strength of the binding in the Zn^+(1,10-phenanthroline) complex suggests that the enhanced polarizability cancels out the steric limitations imposed by 1,10-phenanthroline being planar. The strength of the metal−ligand interaction should also scale with the magnitude of the ligand dipole moment such that stronger binding is expected for ligands with larger dipole moments. Each of the pyridyl rings of 4,4′-dipyridyl is expected to exhibit local dipole moments similar to that of pyridine. Therefore, a similar ion−dipole attraction is expected in Zn^+(pyridine) and Zn^+(4,4′-dipyridyl), consistent with the measured BDEs. The cis conformer of 2,2′-dipyridyl exhibits a larger dipole moment, 3.04 D, and is expected to bind more strongly than *trans*-2,2′-dipyridyl, which is expected to exhibit a local dipole moment similar to that of pyridine (2.31 D), and is only able to interact via one N-donor interaction. Of the ligands examined here, 1,10-phenanthroline exhibits the largest dipole moment, 3.31 D, and the strongest binding interaction.

Both theoretical and experimental results suggest that 1,10-phenanthroline binds slightly more strongly to Zn^+ than 2,2′-dipyridyl. The enhanced binding to 1,10-phenanthroline likely arises as a result of contributions arising from its larger polarizability, its dipole moment, and the lack of hydrogen−hydrogen repulsive interactions that occur in Zn^+(*cis*-2,2′-dipyridyl).

Trends in the Sequential Bond Dissociation Energies. Trends in the sequential BDEs of the $Zn^+(N\text{-L})_x$ complexes examined here are shown in Figure 8. As can be seen in Figure 8, the trends in the sequential BDEs of pyridine and 4,4′-dipyridyl are remarkably similar. Zn^+ forms a very strong bond to the first ligand, but the strength of the binding interactions decreases monotonically with ligation. This trend in the sequential BDEs of these (*N*-L) ligands to Zn^+ differs from that observed for the analogous complexes to Ni^+ and Cu^+.[1,2] In the corresponding $Ni^+(N\text{-L})_x$ and $Cu^+(N\text{-L})_x$ complexes, the BDEs of the first and second ligand are quite strong, but decrease somewhat from the first to the second ligand. A sharp decrease in the BDEs occurs for binding of the third ligand, whereas a fairly small decrease in the BDEs is observed from the third to the fourth ligand.[1,2] The trends in the sequential BDEs of Zn^+ to these *N*-donor ligands can be understood in terms of a balance of several competing factors, the electrostatic ion−dipole and ion−induced dipole attractions, sp polarization of Zn^+, and ligand−ligand repulsion.[53−55] The electrostatic contributions to the binding decrease upon sequential ligation because the effective charge retained by Zn^+ decreases, and the repulsion between ligands increases with the extent of ligation, leading to weaker binding.

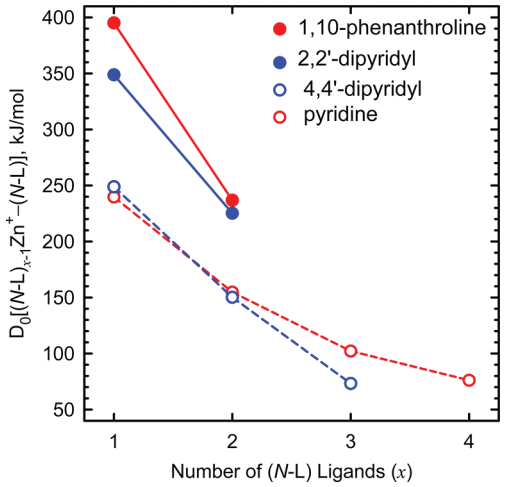

Figure 8. Experimental $(N\text{-L})_{x-1}Zn^+-(N\text{-L})$ BDEs at 0 K (in kJ/mol), where (*N*-L) include 1,10-phenanthroline, 2,2′-dipyridyl, 4,4′-dipyridyl, and pyridine, as a function of the number of (*N*-L) ligands, *x*.

As shown in Figure 8, the measured BDEs for the interaction of Zn^+ to the first ligand are very strong, and are likely enhanced by sp polarization of Zn^+. The electronic configuration of Zn^+ is $4s^13d^{10}$. Therefore, the dσ orbital is occupied. The 4s and 4p orbitals of Zn^+ hybridize to create two new orbitals: a singly occupied orbital oriented 180° away from the ligand and an empty orbital pointing toward the ligand capable of accepting electron density from the nitrogen lone pair. Such hybridization provides a stronger electrostatic interaction by exposing a higher nuclear charge to the ligand. Such sp polarization of Zn^+ allows the first ligand to approach with minimum electronic repulsion, leading to stronger binding. The binding of additional ligands to Zn^+ diminishes the effects of sp polarization, as a result of repulsive interactions between the occupied sp hybridized orbital and the electrons of the ligand.

Evidence for the effects of sp polarization of Zn^+ in these complexes can be found by comparing the first and second BDEs for a variety of complexes to Zn^+ and Na^+. The ratios of the first and second BDEs for the Zn^+ complexes to pyridine, 4,4′-dipyridyl, 2,2′-dipyridyl, and 1,10-phenanthroline are 1.51, 1.66, 1.55, and 1.67, respectively, or, on average, 1.60 ± 0.08. Theory suggests larger relative ratios of 1.95, 2.05, 1.65, and

1.62, respectively, or, on average, 1.82 ± 0.22. In contrast, the ratios of the first and second BDEs for the Na^+ complexes to water,[56] acetonitrile,[57] dimethyl ether,[58] dimethoxyethane,[58] carbon monoxide,[59] and a wide variety of π-ligands[40,46,60−70] are 1.16, 1.17, 1.12, 1.36, 1.33, and 1.19, or, on average, 1.22 ± 0.10. The more significant enhancement in the binding of the first ligand in the Zn^+ complexes arises from sp polarization of Zn^+, which is unimportant for Na^+ because the energetic cost of hybridization exceeds the enhancement in the binding.

The very different trend in the BDEs observed for the analogous complexes to Ni^+ and Cu^+ is due to sd hybridization of these two metal ions. The ground-state electron configurations of isolated Ni^+ and Cu^+ are $4s^03d^9$ and $4s^03d^{10}$, respectively. In these two metal ions, the dσ orbital is half or completely occupied and leads to greater Pauli repulsion between the metal ion and the ligand than when it is unoccupied. In these complexes, the 4s and 3d orbitals hybridize to create two new orbitals: an occupied orbital oriented 90° away from the ligand and an empty orbital pointing toward the ligand for donation by the nitrogen lone pair of electrons. Such sd hybridization effectively removes electron density from the metal−ligand axis by placing the electron density in a hybridized orbital that is perpendicular to the bonding axis, and allows the first two ligands to approach the Ni^+ or Cu^+ center with minimum Pauli repulsion. Therefore, the first two ligands bind much more strongly to these metal ions. The effects of sd hybridization lead to much weaker binding of additional ligands beyond the first two because repulsive interactions with the occupied sd hybridized orbital diminish the effects of sd hybridization.

Binding of the chelating ligands, 2,2′-dipyridyl and 1,10-phenanthroline, to Zn^+ is much stronger than to the analogous monodentate ligands, pyridine and 4,4′-dipyridyl, because the chelating ligands interact with Zn^+ via the lone pairs of electrons of two N atoms. However, the strength of binding in the Zn^+(2,2′-dipyridyl) complex is weaker than the binding of two individual single *N*-donor ligands to Zn^+. In contrast, the Zn^+(1,10-phenanthroline) complex binds slightly more strongly than the sum of the first and second BDEs of pyridine to Zn^+.

The strength of binding of the second ligand to Ni^+ and Cu^+ is nearly equal for all *N*-donor ligands examined here. In contrast, Zn^+ binds the second ligand of 2,2′-dipyridyl and 1,10-phenanthroline more strongly than it does the monodentate ligands, pyridine and 4,4′-dipyridyl. The constrained ligand geometry of the bidentate ligands, greater ligand−ligand repulsion, and the hybridization of the metal ions contribute to these effects. This clearly suggests that the hybridization of the metal ion is most influential in determining the strength of the binding interaction of the second pyridine and 4,4′-dipyridyl ligands.

Trends in the Total BDEs. The trends in the total binding energies of the $Zn^+(N\text{-L})_x$ complexes as a function of the number of N donor atoms interacting with Zn^+ are shown in Figure 9. As can be seen in Figure 9, 4,4′-dipyridyl binds to Zn^+ slightly more strongly than pyridine as a result of its larger polarizability. The sums of the binding energies for the first two pyridine and 4,4′-dipyridyl ligands to Zn^+ are nearly equal (394.5 vs 399.0 kJ/mol) because of the similar binding geometries. However, the sequential BDEs of 4,4′-dipyridyl decrease slightly more rapidly with further ligation than those of pyridine, because ligand−ligand repulsive interactions of the larger 4,4′-dipyridyl ligands overcome the effect of the enhanced polarizability. Hence, the total BDEs for the pyridine

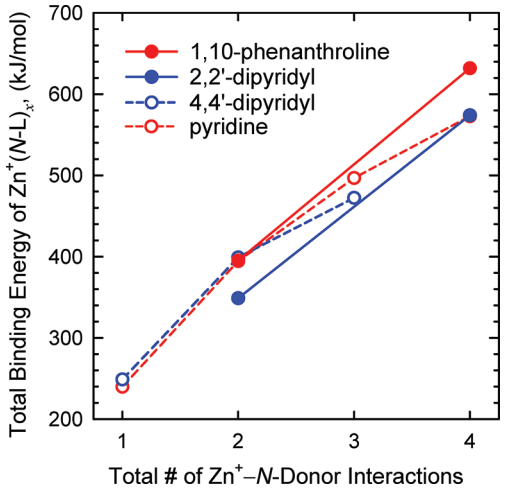

Figure 9. Trends in the measured total BDEs of $Zn^+(N\text{-L})_x$ complexes at 0 K (in kJ/mol) as a function of the number of *N*-donor interactions.

complexes involving more than two ligands slightly exceed those to 4,4′-dipyridyl. The binding interaction of the first 2,2′-dipyridyl ligand to Zn^+ is weaker than the sum of the first and second binding energies of the pyridine and 4,4′-dipyridyl by 45.7 and 50.2 kJ/mol, respectively. However, the binding interaction of the first ligand of 1,10-phenanthroline to Zn^+ is nearly equal to the sum of the first and second BDEs of pyridine, but weaker than 4,4′-dipyridyl by 3.9 kJ/mol. The differences in the strength of the binding interactions observed here are smaller than that observed for Ni^+ and Cu^+ to these ligands. The smaller differences in the binding interactions are the result of the sp polarization of Zn^+ as compared to sd hybridization of Ni^+ and Cu^+, which leads to much stronger binding interactions for the second ligand, but requires a larger ∠NM^+N bond angle of 180° for Ni^+ and Cu^+ versus 120° for Zn^+. 1,10-Phenanthroline binds to Zn^+ slightly more strongly than 2,2′-dipyridyl because of its larger dipole moment and polarizability, and the absence of repulsive H6−H6′ interactions. The second 2,2′-dipyridyl and 1,10-phenanthroline ligands bind to Zn^+ more strongly by 46.9 and 58.5 kJ/mol than the sum of the third and fourth BDEs of pyridine, respectively. This suggests that these chelating ligands experience less ligand−ligand repulsion (two bidentate versus four monodentate ligands) as a result of their constrained ligand geometries.

The total energy required to completely dissociate Zn^+(2,2′-dipyridyl)$_2$ is nearly equal to the total energy required to completely dissociate Zn^+(pyridine)$_4$ into bare Zn^+ and four neutral pyridine ligands. However, the total energy required to completely dissociate Zn^+(1,10-phenanthroline)$_2$ is greater by 59.1 kJ/mol than the total energy required to completely dissociate Zn^+(pyridine)$_4$. In all of these complexes, Zn^+ interacts with the lone pair(s) of electrons of four nitrogen atoms. This suggests that the constrained ligand geometry contributes more to the binding interactions than the ligand−ligand repulsive interactions weaken the binding in the complexes to the flexible pyridine molecules. In contrast, we observed the opposite trend for the analogous complexes to Ni^+ and Cu^+, such that the total energy required to completely dissociate M^+(pyridine)$_4$ into bare M^+ and four neutral pyridine ligands is greater than that required to completely dissociate the

dx.doi.org/10.1021/jp207144b | J. Phys. Chem. A 2012, 116, 1319−1332

$M^+(2,2'\text{-dipyridyl})_2$ and $M^+(1,10\text{-phenanthroline})_2$ complexes.[1,2]

Comparison of Ni^+, Cu^+, and Zn^+ Binding Energies to *N*-donor Ligands. Given the relatively high ionization energy of atomic zinc (9.394 eV),[71] Zn^+ reacts with many neutral molecules through charge transfer to produce ionized ligands $(L)^+$. The IEs of the *N*-donor ligands examined in this study decrease in the order pyridine > 4,4′-dipyridyl > 2,2′-dipyridyl > 1,10-phenanthroline: 9.26 ± 0.01,[38] 9.10 ± 0.02,[38] 8.35 ± 0.02,[38,72] and 8.30 eV,[38,73] respectively. All are lower than the IE of Zn. Consequently, the CID charge transfer formation of $(N\text{-L})^+$ should correspond to the most favorable CID pathway for all of the $Zn^+(N\text{-L})$ complexes, as observed. The competition between the $(N\text{-L})^+$ and Zn^+ channels should increasingly favor the ionized ligand as the IE of $(N\text{-L})$ decreases, as observed. By comparison with the other metal ions previously investigated, closed shell Cu^+ (d^{10}) and open d shell Ni^+ (d^9), Zn^+ (s^1d^{10}) interacts quite differently with these $(N\text{-L})$ ligands.

Besides dative σ-binding and π-back-bonding effects, sd hybridization is found to be of critical importance in the interaction of these *N*-donor ligands with Ni^+ and Cu^+ ions (d^n, n = 9 and 10). Ni^+ and Cu^+ form very strong bonds to the first two ligands as a result of sd hybridization. The binding of more than two ligands to these metal ions diminishes the effects of sd hybridization, resulting in very weak binding of additional ligands. Trends in the sequential BDEs of ligands to Zn^+ ($4s^13d^{10}$) differ from that observed for Ni^+ and Cu^+ (Figure 10a). Zn^+ forms a very strong bond to the first ligand, but binds much more weakly to additional ligands. The sp polarization of Zn^+ allows the first ligand to approach with minimum electronic repulsion. The binding of more than one ligand to Zn^+ diminishes the effect of sp polarization, resulting in weaker binding of additional ligands. The BDEs of these three metal ions follow the order $Ni^+ > Cu^+ > Zn^+$ for the binding to the first and second *N*-donor ligands, such that the more occupied the d and s σ orbitals, the greater the Pauli repulsion and the weaker the binding.

The agreement between B3LYP theory and experiment is roughly parallel for Ni^+ and Cu^+ such that good agreement is observed for the interaction of the first two ligands with both metal ions, but theory systematically underestimates the BDEs when these metal ions interact with more than two ligands. In contrast, reasonably good agreement between the experimentally measured and theoretically calculated BDEs is found for the interaction of Zn^+ with these *N*-donor ligands except for the $Zn^+(\text{pyridine})_2$, $Zn^+(\text{pyridine})_3$, $Zn^+(4,4'\text{-dipyridyl})_2$, and $Zn^+(1,10\text{-phenanthroline})$ complexes, where theory significantly underestimates the BDEs. M06 theory improves the description of most of the $Zn^+(N\text{-L})_x$ systems, but differences still exceed the experimental error in the measurements.

As can be seen in Figure 10b, the binding of the first and second 2,2′-dipyridyl ligands to these metal ions parallel each other and follows the order $Ni^+ > Cu^+ > Zn^+$. Similar results are found for the trends in the binding of 1,10-phenanthroline to these metal ions. The binding strength of the second pyridine and 4,4′-dipyridyl to Ni^+ and Cu^+ is nearly equal to the binding strength of second 2,2′-dipyridyl and 1,10-phenanthroline to these metal ions. The stability gained by the constrained ligand geometry of the chelating ligands is almost canceled by greater ligand−ligand repulsion experienced by the monodentate ligands and results in similar binding strengths for the second chelating and monodentate ligands to these metal ions. In contrast, Zn^+ binds to the second chelating ligand, 2,2′-dipyridyl and 1,10-phenanthroline, more strongly than the monodentate ligands, pyridine and 4,4′-dipyridyl, because the bent bis complexes of the monodentate ligands are under strong steric repulsion compared with linear bis complexes of Ni^+ and Cu^+.

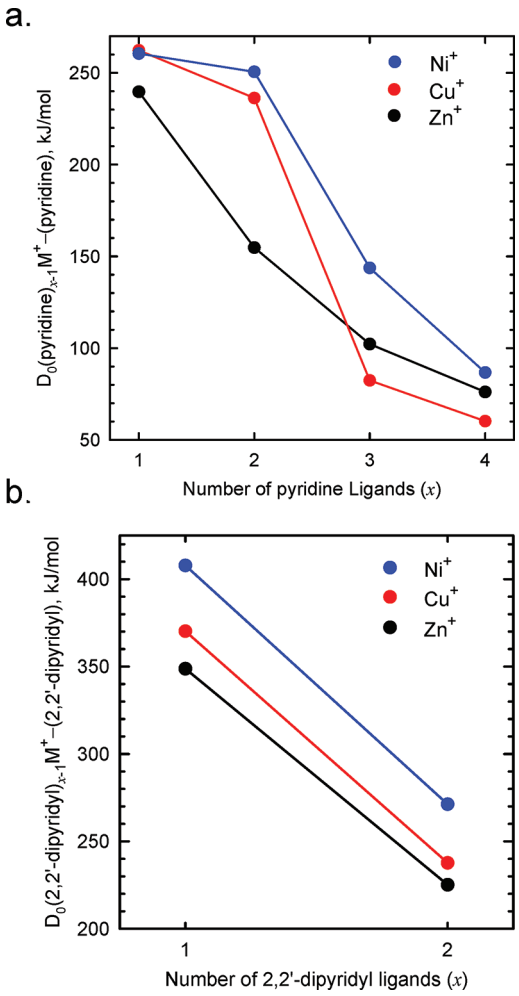

Figure 10. Trends in the experimental $(N\text{-L})_{x-1}M^+-(N\text{-L})$ BDEs, where M^+ = Ni^+, Cu^+, and Zn^+ at 0 K (in kJ/mol) as a function of the number of $(N\text{-L})$ ligands: (a) $(N\text{-L})$ = pyridine; (b) $(N\text{-L})$ = 2,2′-dipyridyl. Values for Ni^+ and Cu^+ are taken from our earlier work.[1,2]

CONCLUSIONS

The gas phase binding interactions of 11 $Zn^+(N\text{-L})_x$ complexes, where $(N\text{-L})$= pyridine (x = 1−4), 4,4′-dipyridyl (x = 1−3), 2,2′-dipyridyl (x = 1−2), and 1,10-phenanthroline (x = 1−2) with Xe are examined in a guided ion beam tandem mass spectrometer. The dominant dissociation processes observed for the monoligated complexes results in formation of the ionized ligand, $(N\text{-L})^+$. In contrast, sequential loss of intact neutral ligands are the major processes observed for the $Zn^+(N\text{-L})_x$ complexes, where x > 1. Thresholds at 0 K for these complexes are determined after consideration of the effects of the reactant internal energy, multiple collisions with Xe, and lifetime effects. The experimental results for all 11 $Zn^+(N\text{-L})_x$ complexes suggest that density functional theory calculations performed at the B3LYP/6-311+G(2d,2p)//B3LYP/6-31G* level of theory systematically underestimate the strength of binding in these systems. M06 theory performs slightly better for some complexes and much better for others, suggesting that

dx.doi.org/10.1021/jp207144b | J. Phys. Chem. A 2012, 116, 1319−1332

this functional is more useful for describing the binding in these systems. Trends in the sequential BDEs of these (*N*-L) ligands to Zn^+ differ from that observed for Ni^+ and Cu^+. Zn^+ forms a very strong bond to the first ligand, which is enhanced by sp polarization of Zn^+, allowing the first ligand to approach with minimum electronic repulsion. The binding of more than one ligand to Zn^+ diminishes the effect of sp polarization, resulting in increasingly weaker binding of additional ligands. The chelating ligands, 2,2′-dipyridyl and 1,10-phenanthroline, exhibit strong binding to Zn^+, but not as strong as to Ni^+ and Cu^+. The strong binding interaction arises as a result of the bidentate interaction and the larger dipole moments and polarizabilities of these ligands.

■ ASSOCIATED CONTENT

Supporting Information

Tables of vibrational frequencies, average vibrational energies at 298 K, rotational constants for the neutral (*N*-L) ligands, and $Zn^+(N\text{-L})_x$ complexes in their ground-state conformations, and enthalpies and free energies of binding of the $Zn^+(N\text{-L})_x$ complexes at 0 and 298 K. Figures showing cross sections for CID of $Zn^+(N\text{-L})_x$ with Xe as well as empirical fits to the primary product channels and total CID cross sections, B3LYP/6-31G* geometry optimized structures of the $Zn^+(4,4'\text{-dipyridyl})_x$ complexes, and the PES for interaction of Zn^+ with 2,2′-dipyridyl. This material is available free of charge via the Internet at http://pubs.acs.org.

■ ACKNOWLEDGMENTS

This work is supported by the National Science Foundation, Grant CHE-0911191. The authors also thank Wayne State University Computing & Information Technology for computer time and support.

■ REFERENCES

(1) Rannulu, N. S.; Rodgers, M. T. *J. Phys. Chem. A* **2007**, *111*, 3465.
(2) Rannulu, N. S.; Rodgers, M. T. *J. Phys. Chem. A* **2009**, *113*, 4534.
(3) Tian, L.; Zhang, W.; Yang, B.; Lu, P.; Ma, Y.; Shen, J. *J. Phys. Chem. B* **2005**, *109*, 6944.
(4) Liu, Y; Li, Y. T.; Schanze, K. S. *J. Photochem. Photobiol.* **2002**, *3*, 1.
(5) Ley, K. D.; Li, Y. T.; Johnson, J. V.; Powell, D. H.; Schanze, K. S. *Chem. Commun.* **1999**, 1749.
(6) Baskar, C.; Lai, Y. H.; Valiyaveettil, S. *Macromolecules* **2001**, *34*, 6255.
(7) Wang, B.; Wasielewski, M. R. *J. Am. Chem. Soc.* **1997**, *119*, 3519.
(8) Chen, L. X.; Jager, W. J. H.; Gosztala, D. J.; Niemczyk, M. P.; Wasielewski, M. R. *J. Phys. Chem. B* **2000**, *104*, 1950.
(9) Tian, L. L.; Zhang, M.; Lu, P.; Zhang, W.; Yang, B.; Ma, Y. G. *Chin. Sci. Bull.* **2004**, *49*, 246.
(10) Manas, E. S.; Chen, L. X. *Chem. Phys. Lett.* **2000**, *331*, 299.
(11) Zhang, M.; Lu, P.; Ma, Y. G.; Shen, J. C. *J. Phys. Chem. B* **2003**, *107*, 6535.
(12) Wang, Y.; Quillian, B.; Wei, P.; Wang, H.; Yang, X.-J.; Xie, Y.; King, R. B.; Schleyer, P. v. R.; Schaefer, H. F. III; Robinson, G. H. *J. Am. Chem. Soc.* **2005**, *127*, 11944.
(13) Grirrane, A.; Resa, I.; Rodriguez, A.; Carmona, E.; Alvarez, E.; Gutierrez-Puebla, E.; Monge, A.; Galindo, A.; del Río, D.; Andersen, R. A. *J. Am. Chem. Soc.* **2007**, *129*, 693.
(14) Schulz, S.; Schuchmann, D.; Westphal, U.; Bolte, M. *Organometallics* **2009**, *28*, 1590.
(15) Nelson, R. D.; Lide, D. R.; Maryott, A. A. *Selected Values of Electric Dipole Moments for Molecules in the Gas Phase*; National Standard Reference Data Series (U. S., National Bureau of Standards) 10; National Bureau of Standards: Washington, DC, 1967.
(16) Rodgers, M. T.; Ervin, K. M.; Armentrout, P. B. *J. Chem. Phys.* **1997**, *106*, 4499.
(17) Rodgers, M. T. *J. Phys. Chem. A* **2001**, *105*, 2374.
(18) Teloy, E.; Gerlich, D. *Chem. Phys.* **1974**, *4*, 417.
(19) Dalleska, N. F.; Honma, K.; Armentrout, P. B. *J. Am. Chem. Soc.* **1993**, *115*, 12125.
(20) Aristov, N.; Armentrout, P. B. *J. Phys. Chem.* **1986**, *90*, 5135.
(21) Hales, D. A.; Armentrout, P. B. *J. Cluster Sci.* **1990**, *1*, 127.
(22) Ervin, K. M.; Armentrout, P. B. *J. Chem. Phys.* **1985**, *83*, 166.
(23) Dalleska, N. F.; Honma, K.; Sunderlin, L. S.; Armentrout, P. B. *J. Am. Chem. Soc.* **1994**, *116*, 3519.
(24) Frisch, M. J.; Trucks, G. W.; Schlegel, H. B.; Scuseria, G. E.; Robb, M. A.; Cheeseman, J. R.; Montgomery, J. A., Jr.; Vreven, T.; Kudin, K. N.; Burant, J. C.; Millam, J. M.; Iyengar, S. S.; Tomasi, J.; Barone, V.; Mennucci, B.; Cossi, M.; Scalmani, G.; Rega, N.; Petersson, G. A.; Nakatsuji, H.; Hada, M.; Ehara, M.; Toyota, K.; Fukuda, R.; Hasegawa, J.; Ishida, M.; Nakajima, T.; Honda, Y.; Kitao, O.; Nakai, H.; Klene, M.; Li, X.; Knox, J. E.; Hratchian, H. P.; Cross, J. B.; Bakken, V.; Adamo, C.; Jaramillo, J.; Gomperts, R. R.; Stratmann, E.; Yazyev, O.; Austin, A. J.; Cammi, R.; Pomelli, C.; Ochterski, J. W.; Ayala, P. Y.; Morokuma, K.; Voth, G. A.; Salvador, P.; Dannenberg, J. J.; Zakrzewski, V. G.; Dapprich, S.; Daniels, A. D.; Strain, M. C.; Farkas, O.; Malick, D. K.; Rabuck, A. D.; Raghavachari, K.; Foresman, J. B.; Ortiz, J. V.; Cui, Q.; Baboul, A. G.; Clifford, S.; Cioslowski, J.; Stefanov, B. B.; Liu, G.; Liashenko, A.; Piskorz, P.; Komaromi, I.; Martin, R. L.; Fox, D. J.; Keith, T.; Al-Laham, M. A.; Peng, C. Y.; Nanayakkara, A.; Challacombe, M.; Gill, P. M. W.; Johnson, B.; Chen, W.; Wong, M. W.; Gonzalez, C. Pople, J. A. *Gaussian 03*, revision C.01; Gaussian, Inc.: Wallingford, CT, USA, 2004.
(25) Becke, A. D. *J. Chem. Phys.* **1993**, *98*, 5648.
(26) Lee, C.; Yang, W.; Parr, R. G. *Phys. Rev. B* **1988**, *37*, 785.
(27) Foresman, J. B.; Frisch, A. E. *Exploring Chemistry with Electronic Structure Methods*, 2nd ed.; Gaussian: Pittsburgh, PA, USA, 1996; p 64.
(28) Boys, S. F.; Bernardi, R. *Mol. Phys.* **1979**, *19*, 553.
(29) van Duijneveldt, F. B.; van Duijneveldt-van de Right, J. G. C. M.; van Lenthe, J. H. *Chem. Rev.* **1994**, *94*, 1873.
(30) Muntean, F.; Armentrout, P. B. *J. Chem. Phys.* **2001**, *115*, 1213.
(31) Beyer, T. S.; Swinehart, D. F. *Commun. ACM* **1973**, *16*, 379.
(32) Stein, S. E.; Rabinovitch, B. S. *J. Chem. Phys.* **1973**, *58*, 2438.
(33) Pople, J. A.; Schlegel, H. B.; Raghavachari, K.; DeFrees, D. J.; Binkley, J. F.; Frisch, M. J.; Whitesides, R. F.; Hout, R. F.; Hehre, W. J. *Int. J. Quant. Chem., Symp.* **1981**, *15*, 269.
(34) Khan, F. A.; Clemmer, D. E.; Schultz, R. H.; Armentrout, P. B. *J. Phys. Chem.* **1993**, *97*, 7978.
(35) Chesnavich, W. J.; Bowers, M. T. *J. Phys. Chem.* **1979**, *83*, 900.
(36) Armentrout, P. B.; Simons, J. *J. Am. Chem. Soc.* **1992**, *114*, 8627.
(37) Rodgers, M. T.; Armentrout, P. B. *J. Chem. Phys.* **1998**, *109*, 1788.
(38) Lias, S. G. Ionization Energy Evaluation. In *NIST Chemistry WebBook*; Lindstrom, P. J., Mallard, W. G., Eds.; NIST Standard Reference Database Number 69; National Institute of Standards and Technology: Gaithersburg, MD, USA, 2005. http://webbook.nist.gov.
(39) Rodgers, M. T.; Armentrout, P. B. *Mass Spectrom. Rev.* **2000**, *19*, 215.
(40) Amunugama, R.; Rodgers, M. T. *J. Phys. Chem. A* **2001**, *105*, 9883.
(41) Rodgers, M. T.; Armentrout, P. B. *J. Phys. Chem. A* **1999**, *103*, 4955.
(42) LeFevre, C. G.; LeFevre, R. J. W.; Rao, B. P.; Smith, M. R. *J. Chem. Soc.* **1959**, 1188.
(43) Sanyal, N. K.; Ahmad, P.; Dixit, L. *J. Phys. Chem.* **1973**, *77*, 2552.
(44) Adams, S.; Nir, S.; Rein, R. *Int. J. Quantum Chem.* **1975**, *9*, 701.
(45) Rodgers, M. T.; Stanley, J. R.; Amunugama, R. *J. Am. Chem. Soc.* **2000**, *122*, 10969.
(46) Amunugama, R.; Rodgers, M. T. *Int. J. Mass. Spectrom.* **2000**, *195/196*, 439.
(47) Rodgers, M. T.; Armentrout, P. B. *Int. J. Mass. Spectrom.* **1999**, *185/186/187*, 359.

(48) Rannulu, N. S.; Amunugama, R.; Yang, Z.; Rodgers, M. T. *J. Phys. Chem. A* **2004**, *108*, 6385.
(49) McKenna, A. G.; McKenna, J. F. *J. Chem. Educ.* **1984**, *61*, 771.
(50) Rue, C.; Armentrout, P. B.; Kretzschmar, I.; Schroder, D.; Schwarz, H. *J. Phys. Chem. A* **2002**, *106*, 9788.
(51) Rodgers, M. T.; Armentrout, P. B. *J. Am. Chem. Soc.* **2002**, *124*, 2678.
(52) Ruan, C.; Rodgers, M. T. *J. Am. Chem. Soc.* **2009**, *131*, 10918.
(53) Bauschlicher, C. W.; Langhoff, S. R.; Partridge, H. *J. Chem. Phys.* **1991**, *94*, 2064.
(54) Bauschlicher, C. W.; Langhoff, S. R.; Partridge, H. *J. Phys. Chem.* **1992**, *96*, 3273.
(55) Langhoff, S. R.; Bauschlicher, C. W.; Partridge, H. *J. Phys. Chem.* **1991**, *95*, 10667.
(56) Amicangelo, J. C.; Armentrout, P. B. *Int. J. Mass Spectrom.* **2001**, *212*, 301.
(57) Valina, A. B.; Amunugama, R.; Huang, H.; Rodgers, M. T. *J. Phys. Chem. A* **2001**, *105*, 11057.
(58) More, M. B.; Ray, D.; Armentrout, P. B. *J. Phys. Chem. A* **1997**, *101*, 831.
(59) Walter, D.; Sievers, M. R.; Armentrout, P. B. *Int. J. Mass Spectrom.* **1998**, *175*, 93.
(60) Amunugama, R.; Rodgers, M. T. *J. Phys. Chem. A* **2002**, *106*, 5529.
(61) Amunugama, R.; Rodgers, M. T. *J. Phys. Chem. A* **2002**, *106*, 9092.
(62) Amunugama, R.; Rodgers, M. T. *J. Phys. Chem. A* **2002**, *106*, 9718.
(63) Amunugama, R.; Rodgers, M. T. *Int. J. Mass Spectrom.* **2003**, *222*, 431.
(64) Amunugama, R.; Rodgers, M. T. *Int. J. Mass Spectrom.* **2003**, *227*, 1.
(65) Amunugama, R.; Rodgers, M. T. *Int. J. Mass Spectrom.* **2003**, *227*, 339.
(66) Ruan, C.; Rodgers, M. T. *J. Am. Chem. Soc.* **2004**, *126*, 14600.
(67) Ruan, C.; Yang, Z.; Hallowita, N.; Rodgers, M. T. *J. Phys. Chem. A* **2005**, *109*, 11539.
(68) Ruan, C.; Yang, Z.; Rodgers, M. T. *Int. J. Mass Spectrom.* **2007**, *267*, 233.
(69) Hallowita, N.; Carl, D. R.; Armentrout, P. B.; Rodgers, M. T. *J. Phys. Chem. A* **2008**, *112*, 7996.
(70) Hallowita, N.; Udonkang, E.; Ruan, C.; Frieler, C. E.; Rodgers, M. T. *Int. J. Mass Spectrom.* **2009**, *283*, 35.
(71) Brown, C. M.; Tilford, S. G.; Ginter, M. L. *J. Opt. Soc. Am.* **1975**, *65*, 1404.
(72) Maier, J. P.; Turner, D. W. *Faraday Discuss. Chem. Soc.* **1972**, *54*, 149.
(73) Hush, N. S.; Cheung, A. S.; Hilton, P. R. *J. Electron Spectrosc. Relat. Phenom.* **1975**, *7*, 385.